The Binding Potential between the Cholera Toxin B-Oligomer and Its Receptor[†]

Xian-E Cai and Jie Yang*

Physics Department, University of Vermont, Cook Building, Burlington, Vermont 05405

Received October 16, 2002; Revised Manuscript Received February 17, 2003

ABSTRACT: Employing atomic force microscopy as an in situ molecular force probe, we have measured the binding strength between cholera toxin B-pentamer (ctB) and its membrane receptor, ganglioside G_{M1}. By application of the basic principle of the reaction rate theory, key parameters of the ligand−receptor binding potential can be obtained from our data. The potential has a well with a spatial span of about 2.5 Å and a depth of at least six times the thermal energy at room temperature. The very short range nature of the binding potential leads to the specificity of the ctB−G_{M1} coupling.

Formation and dissociation of chemical compounds have been well characterized by the reaction rate theory following the pioneer work by Kramers (*1*). Ligand−receptor bindings in biological systems are special cases of compound formation and should be governed by the reaction rate theory. We have used atomic force microscopy (AFM) to investigate the binding between cholera toxin B-pentamer (ctB) and its receptor, ganglioside G_{M1}. Analyzing a large number of force curves automatically, we obtained a distribution function of the ligand−receptor bond for the ctB−G_{M1} compound. On the basis of the reaction rate theory, the distribution function indicates that the binding potential for the ctB−GM1 compound has a spatial span of about 0.25 nm and a depth of at least six times the thermal energy at room temperature.

Cholera toxin has been extensively studied over the past several decades because of its profound effect in causing massive diarrhea, a devastating disease that causes water to flow from the blood through epithelial cells into the small intestine (*2*, *3*). This toxin has the A-B structure seen in many bacterial toxins, with the A-subunit catalytically active and B-subunits (ctB pentamer) responsible for the binding to the membrane receptor (a ganglioside, G_{M1}) (*4*, *5*). The doorway for the toxin to attack a host cell is the strong binding of the ctB pentamer to the cell membrane where receptors are naturally hosted. Although biochemical studies have determined the dissociation constant for the ctB−G_{M1} compound, ranging from 4.6×10^{-12} M with a surface plasma resonance BIAcore apparatus (*6*) to about 10^{-9} M in earlier cell assay studies (*7*) and 2.5×10^{-8} M according to surface spectroscopic measurements (*8*), the molecular basis of the binding process has not been established. An understanding of the molecular details of the binding process may help to establish an efficient means to allow certain cells to fend off the devastating offense by the toxin or to use the toxin to attack selected cell types, such as cancer cells. X-ray diffractional studies have identified the structure of the binding pocket of ctB (*9*, *10*), providing an essential insight to the microscopic nature of the ctB−G_{M1} coupling.

Atomic force microscopy has shown great potential in biological applications, ranging from high-resolution structural studies (*11*) to the investigation of macromolecular interactions. As a sensitive force probe, AFM has been used to determine the binding strength of the covalent bond (*12*), ligand−receptor attraction between biotin, its derivatives, and their corresponding conjugates (*13*), the hydrogen bond strength (*14*, *15*), and the binding between complementary strands of DNA (*16*). AFM has also been used to investigate the elastic properties of sugar backbones (*17*). Recently, Evans has proposed a model to postulate a dynamic nature of noncovalent bonds on the basis of the reaction rate theory and showed the consistency of the model to the biotin−streptavidin bond in their experiments using the biomembrane force probe (BFP) (*18*).

A major task using AFM as a molecular force probe is to treat the tip so that the detected force represents the strength of a specific intermolecular bond. Our success in probing the molecular bond strength of the ctB−G_{M1} compound lies in the development of a method that treated an AFM tip to allow covalent attachment of ctB at the very tip with the receptor-binding site still available. Our results provide, for the first time, an elucidation of the molecular nature of the binding process of the ctB−G_{M1} compound. We also show that, for the ctB−G_{M1} bond in the time scale of milliseconds to 0.1 s, the bond strength distribution function is described by a static limit of a very slow dynamic process with the bond formation governed by the reaction rate theory.

MATERIALS AND METHODS

Materials. Ganglioside G_{M1} (catalog no. G-7641) and ctB pentamers (catalog no. C-9903) were obtained from Sigma-Aldrich as lyophilized powder and used after dilutions. Lipids of egg yolk phosphatidylcholine (egg PC) were obtained from Avanti Polar Lipids (Alabaster, AL). All chemicals and salts were also obtained from Sigma-Aldrich.

Force Probe. Force curves were obtained in 20 mM NaCl with a nanoscope E AFM from Digital Instruments (Santa Barbara, CA). Typical pH values in the solution were about 6.5−7, without introducing large organic buffering ions. With in situ AFM experiments, the fluid cell is filled with pure

[†] Partially supported by the Army Research Office.

* Corresponding author. Phone: (802) 656-0061. Fax: (802) 656-0817. E-mail: Jie.Yang@uvm.edu.

10.1021/bi027016h CCC: $25.00
Published on Web 03/21/2003

solutions without any constituent to cause a significant change in the concentration of H^+ ions and, hence, the pH value. Thus, the buffering is not as important as in the incubation procedures where proper buffers (described later) were used. Force curve data were converted to ASCII format for analysis.

Substrate. Egg PC bilayers were prepared as described earlier (*19*). Gangliosides (G_{M1} at 95% purity) were incorporated into a bilayer by incubation at a concentration of 0.05 mM for 1 h at room temperature, and extra gangliosides were removed by thorough solution exchanges.

AFM Imaging and Sample Characterization. The integrity of ctB pentamers was characterized using direct AFM imaging in solution. For a receptor-incorporated bilayer in a buffer containing 0.12 mM Tris, 20 mM NaCl, and 0.0024 mM EDTA, pH 7.5, ctB pentamers were introduced at a concentration of 0.0002 mM. The incubation lasted several hours at room temperature and then continued overnight at 4 °C. The incubation bubble had a volume of about 0.3 mL. After the incubation, the sample was washed with 20 mM NaCl, and then images were obtained in 20 mM NaCl. The above procedure usually resulted in closely packed membrane-bound ctB pentamers as seen with in situ AFM imaging (a typical example is shown in Figure 3). However, for pure bilayers without incorporated receptors, the same procedure of incubation with ctB did not result in any adsorption of ctB to the bilayer. The fluidity of the bilayer is also essential for the incorporation of sufficient receptors into the bilayer. We have tried to incorporate receptors at 0.05 mM in bilayers of other lipid species in the gel phase for 1 h at room temperature and did not detect any incorporated receptor with in situ AFM imaging using ctB as the labeling protein, employing the same ctB incubation procedure. This is in sharp contrast to the closely packed labeling ctB when receptors were incubated with fluid phase bilayers. The high quality of closely packed ctB in AFM images shows the integrity of the protein. The fact that ctB only bound to receptor-incorporated bilayers demonstrated the specificity of the binding and thus the good activity of these ctB pentamers. Because supported bilayers have only slightly higher main phase transition temperatures than normal lamellar bilayers (*20*), our results also showed the importance of the fluidity for efficient receptor incorporation.

Tip Treatment. Our method stems from the well-developed protocol of treating the inner wall of a glass capillary tube to eliminate the electroosmotic flow in capillary electrophoresis of DNA molecules (*21*). Residue oxides of an oxide-sharpened silicon nitride tip facilitated the silanization of the tip with (methacryloxypropyl)trimethoxysilane (MAPS). Ammonium persulfate (APS) initiated opening of the alkene double bond of the MAPS to allow a covalent attachment of a reactive residue of the ctB, with *N*,*N*,*N*′,*N*′-tetramethylethylenediamine (TEMED) as a catalyst. Therefore, if a MAPS-silanized tip is exposed to ctB pentamers in the presence of the catalytic agents APS and TEMED, ctB can be attached to the tip. The treatment started by first applying a drop of MAPS on a fresh oxide-sharpened silicon nitride tip and letting the tip dry briefly. Then, the silanized tip was immersed in a buffer (0.5 mM Tris, 22 mM NaCl, 0.03 mM NaN_3, 0.01 mM EDTA, pH 7.5) containing ctB at a concentration of 0.01 mg/mL for 30 min. While being incubated, APS and TEMED were introduced as droplets at a very low final concentration of 0.01%. Immediately after the treatment the tip was swiftly transferred to a cell containing a G_{M1}-incorporated bilayer to obtain force curves, and the tip remained hydrated through the process. The swift transfer and the low concentration of APS helped to minimize any effect the APS may have on an attached ctB. Not all such prepared tips showed binding to G_{M1}-incorporated supported bilayers. Those that showed the binding were used for our study, and the binding was specific since so treated tips did not show binding to bilayers without any receptor (see Figure 2b). Those that did not show any binding could be due to several scenarios, such as the lack of a free ctB in the vicinity of the tip, an attached ctB at a nonpreferred orientation, or even that APS occasionally might have some effect on the binding efficiency of ctB. By no means is the above list complete, but for our purpose we only worked with those treated tips showing ctB−G_{M1} binding characteristics.

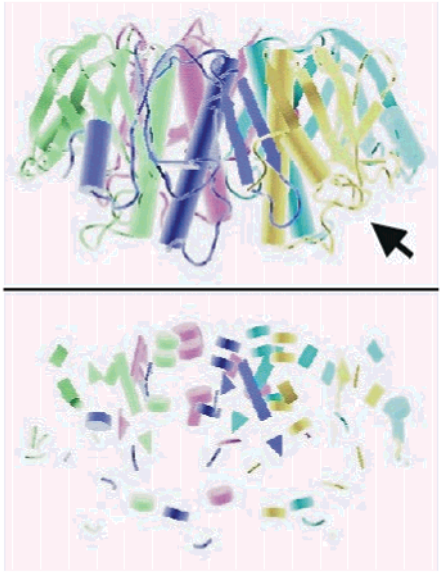

FIGURE 1: Cartoon representation of the 3-D structure of ctB in a side view, with the upper part the ctB pentamer and the lower part the positions of S, T, and Y residues. The five colors represent the five B-subunits. The VMD program downloaded from the UIUC Theoretical Biophysics Group generated the two pictures (http://www.ks.uiuc.edu).

RESULTS

The basis for the attachment with the receptor-binding site available lies in the structure of ctB itself (*9*, *10*). Figure 1 shows a cartoon view of the ctB pentamer in the top panel. The arrow points to the receptor-binding pocket for one subunit. The bottom panel shows the positions of the three reactive residues (S, T, and Y) of ctB. It is seen that the density of reactive residues is much higher at the top of the molecule. Then, it is likely to attach ctB to a MAPS-silanized tip at those top reactive residues with the binding pocket available, allowing the attached ctB to catch receptors incorporated in a fluid-phase lipid bilayer.

A typical force curve to measure the binding strength is shown in Figure 2a, where the baseline is set as zero with attraction negative and repulsion positive. The maximum magnitude of the attractive force is the binding strength before the tip snaps to detachment from the sample surface.

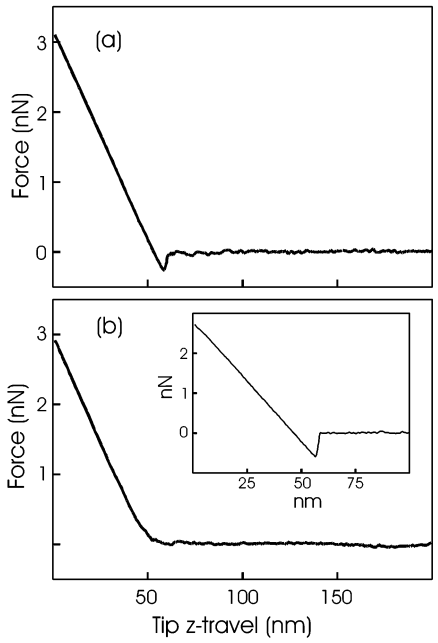

FIGURE 2: Part a shows a typical force curve obtained with a ctB-attached tip on a bilayer of egg PC containing the receptor G_{M1}. Part b shows a force curve by a similarly treated tip on a bilayer of pure egg PC, with no sign of any binding activity. The insert in (b) shows that the same treated tip in (b) did show a significant binding on a G_{M1}-incorporated egg PC bilayer.

The binding of ctB to G_{M1} has been known to be noncovalent, as also supported by the X-ray structure of the binding pocket. Therefore, it is likely that electrostatic and van der Waals forces play the main role for the affinity. However, our force curves showed that the binding lacks any long-range character, indicating that there must exist substantial screening, similar to a number of cases where screened electrostatic interaction mediates interaction among biomacromolecules (*22*, *23*). Figure 2b shows a force curve without any tip−sample attraction with a treated tip on pure egg PC bilayers, indicating that the binding is receptor-specific. The same tip did show significant binding on a receptor-incorporated bilayer (see the insert in Figure 2b).

The receptor ganglioside G_{M1}, which is a lipid molecule (*24*), was incorporated into a supported egg yolk phosphatidylcholine (egg PC) bilayer via direct incubation of the bilayer with a solution containing G_{M1} at a concentration of 0.05 mM, well above the CMC of G_{M1} (*25*). The incorporation of the receptor into the bilayer was assured experimentally by examining such prepared surfaces using ctB pentamers as labeling proteins with in situ AFM in the contact mode. It was found that bound ctBs on a G_{M1}-incorporated egg PC bilayer were closely packed, as shown in Figure 3. The high-resolution image was very stable against repeatable scanning regardless of the fact that bound ctB pentamers were on a fluid-phase egg PC bilayer. AFM imaging in the contact mode, even operated in solution, still applied significant force (about 0.1 nN) on the sample (*11*). Thus, all five binding sites of the ctB pentamer must be bound to receptors for the sample to sustain the lateral probe drag in AFM imaging. If all incorporated gangliosides were bound to ctB, the ratio of gangliosides to PC lipids is close to 10%, according to the headgroup sizes of the two lipids (*9*, *26*). Thus, it is highly likely that the surface coverage of incorporated gangliosides is at an even higher percentage.

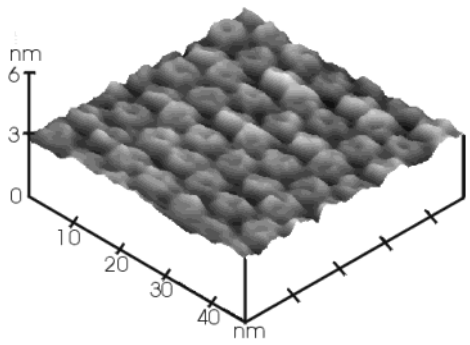

FIGURE 3: AFM image obtained in 20 mM NaCl of membrane-bound ctB on a G_{M1}-incorporated egg PC bilayer in a surface plot with well-resolved individual pentamers.

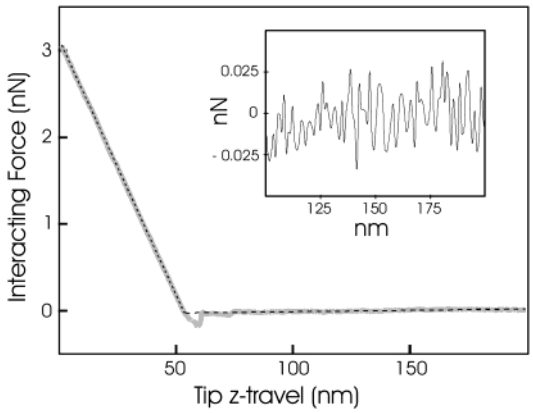

FIGURE 4: Graph showing our method to automate the determination of the binding strength. Two linear fits (dark dashed lines) coincide mostly with the force curve (in light shadow) except in the region around the tip−sample contact point. The insert shows a typical example of the noise level of a force curve baseline.

Our method of incorporating G_{M1} into a planar bilayer has the advantage of using a much smaller amount of materials for the purpose. It is possible to mix G_{M1} with lipids initially before the process of bilayer preparation so that the concentration of G_{M1} might actually be determined, assuming perfect miscibility, and that the process of planar bilayer formation may not alter the mixing. However, in that case a large number of G_{M1} molecules would be required, and it is likely that the process of planar bilayer formation actually alters the mixing because of a strong lipid−substrate interaction. This interaction makes it intrinsically difficult to determine the concentration of incorporated G_{M1} molecules with other analytical methods so that our estimation of the receptor concentration on the basis of surface density of bound ctB at least provides a valid lower limit.

Since AFM is an extremely localized force probe, it is equally important to record a great number of force curves to achieve enough statistical significance. For this purpose, we wrote a program facilitating automatic analysis of a large number of force curves to avoid artificial error. Figure 4 shows our method. Two linear fits to both the slope and the baseline were first obtained. Then, the program calculated the difference between the force curve and the fitting lines and assigned the maximum adhesion force as the binding strength before the bond breakage. The main error for the above procedure lies on the limit of the instrument, which can be obtained by examining the noise level of the baseline. The insert in Figure 4 is a typical baseline, demonstrating

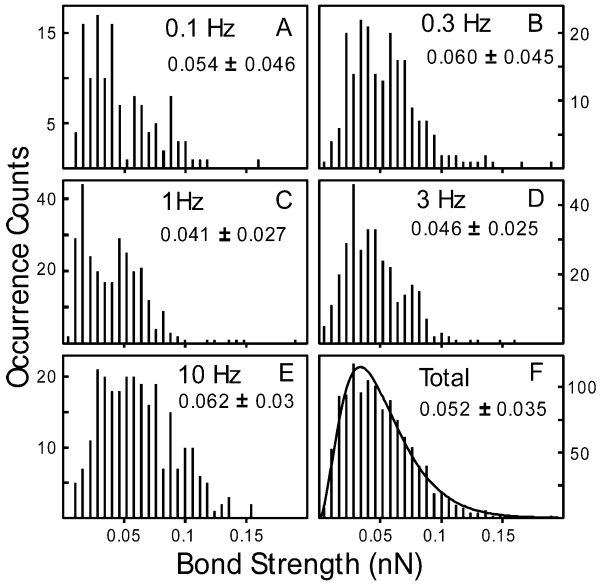

FIGURE 5: Histograms of measured binding strength (in nN) normalized between a ctB monomer and its receptor ganglioside G_{M1} in 20 mM NaCl at the vertical raster frequencies shown (A−E). The fit in part F is of the functional form $(3 \times 10^4)F^2 \exp(-0.25F/k_BT)$, with F in nN, 0.25 in nm, and a 3×10^4 prefactor. The average value and the standard deviation for each case are given in nN.

the noise level of our force measurements. An average of 202 baselines resulted in an average of an absolute base amplitude of 0.017 ± 0.013 nN, leading to our force measurements in units of 0.03 nN.

Figure 5 summarizes our results. In our experiments, the tip-attachment reaction time was reduced to a minimum. At the final adopted condition, not all treated tips showed the adhesion force. Therefore, our measured bond strength corresponds to that of a ctB pentamer. For a single ctB−G_{M1} bond, the strength is one-fifth the detected value. Bond strengths were obtained at five vertical raster frequencies (10, 3, 1, 0.3, and 0.1 Hz). Judging from the standard deviation at each frequency, our results indicate that, in the time scale of our experiments that covered a span of two decades, no systematic frequency dependency of the bond strength was observed. In our force curves only about one-tenth of the time was the tip in contact with the sample (see Figure 2). Therefore, the binding must have established a quasi-static dynamic equilibrium in less than 10 ms because the fastest frequency of our experiments was 10 Hz.

Combining our results for all of the five frequencies resulted in a large number of data to obtain a statistically significant histogram of the bond strength for a single ctB−G_{M1} bond. The distribution function fits well to a functional form of $\beta F^2 \exp(-\alpha F/k_BT)$, with β and α two constants. This may allow a better understanding of the physical mechanism of the binding process. The main character of the distribution function is an asymmetric pattern with a long shoulder at the higher force side, markedly different from a recent theoretical investigation of single bond dynamics where an asymmetric distribution of bond strength had a long shoulder at the lower force end (*27*, *28*).

DISCUSSION

The process of binding and unbinding is intrinsically a chemical reaction with the rates of dissociation and recombination governed by the reaction kinetics, and the reaction rate theory has been well developed following pioneer work by Kramers (*1*). For the ctB−G_{M1} association, the binding potential energy U as a function of the ligand−receptor distance must have a well and a barrier, as illustrated in Figure 6. The depth of the well ($E_b - E_a$) governs the rate of binding, and the height of the barrier (E_b) determines the difficulty to initiate the binding. The distribution function of the binding strength allows us to deduce a value of the microscopic spatial paramer, $(b - a) = 0.25$ nm. On the basis that the binding of ctB to its receptor is quite strong (*7*), it is likely that the barrier is low and the depth is deep. Our experimental results also lead to a lower limit of potential well depth of about six times the thermal energy at room temperature.

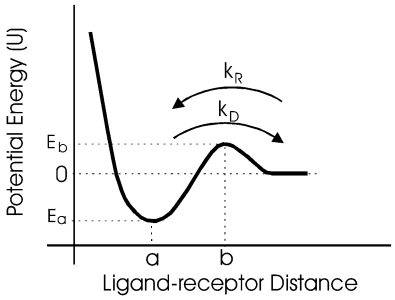

FIGURE 6: Illustration of the attractive potential responsible for the binding of ctB to its receptor G_{M1}. The horizontal axis is the distance between ctB and its receptor and the vertical axis is the potential energy U. The dissociation rate k_D and the recombination rate k_R are shown at the top of the potential barrier.

To analyze our experimental situation, we realize that the binding and the dissociation of the ctB−G_{M1} compound are characterized by the dissociation and recombination rates (k_D and k_R in Figure 6; note that the dissociation rate is not the same as the dissociation constant). According to the reaction rate theory, at equilibrium we have

$$n_a = n_d(k_R/k_D) \tag{1}$$

with $k_R \propto \exp[-E_b/k_BT]$ and $k_D \propto \exp[(E_a - E_b)/k_BT]$, and E_a negative, with n_a the probability that the compound stays bound and n_d the probability of the two being separated.

An external force (F) changes the energy landscape of the binding potential and affects both of the rates, k_D and k_R. Then, the bound state is no longer a true thermal equilibrium state, and the compound must eventually dissociate. However, there is a time scale for the dissociation to occur. If that time scale is rather long, we can then approximate the situation as the force only affecting the two rates, k_D and k_R. In this static approximation of a rather long dynamic process, the major effect of the force on the two rates is a change of the Arrhenius exponential factor, with $k_{DF} = k_D \exp[F(b - a)/k_BT]$ and $k_{RF} = k_R \exp[-F(x - b)/k_BT]$, leading to an increase of the dissociation rate and a decrease of the recombination rate and resulting in a probability

$$n_{aF} = n_a \exp[-F(x - a)/k_BT] \tag{2}$$

When $x > b$, any recombination is actually unlikely, so that the above approximation is only valid for x larger than but in very close vicinity of b. Then, in the static approximation limit we have

$$n_{aF} = n_a \exp[-F(b - a)/k_BT] \tag{3}$$

The physical meaning of the static approximation is that, under an external force F, the bond cannot be stretched more than the spatial span of the potential well for the compound to stay intact and that the depth of the potential well is reduced by a factor of $\exp[-F(b - a)/k_BT]$.

Within the potential well, the compound behaves like an oscillator, and the application of a force F causes the system's energy to increase by an amount proportional to F^2. a similar conclusion can also be drawn if one considers the collision model where the force F causes an increase (decrease) in velocity ($\Delta\upsilon$) of a particle as it bounces back and forth within the potential well, with $\Delta\upsilon$ proportional to the force F according to the Newtonian mechanics. This process results in a net increase of the kinetic energy proportional to $\Delta\upsilon^2$ and, hence, proportional to F^2. Realizing that the probability for ctB bound to G_{M1} is n_{aF}, we see that the actual energy delivered to the system by an applied force F is therefore proportional to $n_{aF}F^2$. Thus, the external force causes an increase of the compound's free energy by ΔE that is proportional to $n_{aF}F^2$. According to statistical physics, the probability of compound breaking is then proportional to $[1 - \exp(-\Delta E/k_BT)]$, which is directly proportional to ΔE in the limit of small ΔE.

The distribution function of the binding strength is a direct map of the bond breakage probability. Remarkably, the experimental distribution fits well to the functional form of $\beta F^2 \exp(-\alpha F)$, as seen in Figure 5F. Our fit results in a spatial parameter of the potential well, with $(b - a) = 0.25$ nm. The depth ($-E_a$) of the original potential well is difficult to determine solely from the distribution function. However, a reasonable estimate can be made according to our data. Numerical solution shows that the distribution function reduces to 1/e of its maximum value at $F_e(b - a)/k_BT = 4.7$, corresponding to $F_e(b - a) = 4.7k_BT$. This value is the net reduction of the original potential depth ($-E_a$) by the applied force. Because the distribution function is only 1/e of the maximum under the applied force F_e, it is reasonable to assume that the well still exists and it must be at least of the order of the thermal energy k_BT. Then, the minimum depth of the original potential well ($-E_a$) should be about six times the thermal energy at room temperature.

We can also obtain a lower limit of the bond spring constant according to the above energetic estimation. Assuming a parabolic potential profile smoothly rises over to the barrier, we obtain

$$(1/2)k[(b - a)/2]^2 = 6k_BT/2 \qquad (4)$$

with k the spring constant of the ctB$-G_{M1}$ bond, resulting in a k of about 1.6 N/m. According to Figure 5F, the maximum of the bond strength distribution function is at 0.034 nN, so that the corresponding stretch of the bond is about 0.02 nm. The depth of $6k_BT$ is a lower estimation and, hence, the spring constant k so obtained is also a lower limit. Thus, the actual stretching of the ctB$-G_{M1}$ bond can be even smaller, well below the spatial span of the potential well. This condition favorably supports the validity of the static limit approximation, since the delivered energy to the system is much smaller than the depth of the potential well.

With the estimated spring constant, we can obtain a rough analysis of the attempt frequency, which is of the order of $\sqrt{k/M_{eff}}/2\pi$, with M_{eff} an effective mass. For a bare ctB$-G_{M1}$ bond with the G_{M1} in a bilayer, M_{eff} is essentially the mass of a ctB monomer. For a tip-attached ctB, the effective mass also includes the mass of the tip, and even the mass of the bilayer is no longer necessarily larger because the mass of the tip is macroscopic. Then, the effective mass can be very large, leading to a very slow attempt frequency. This would lead to a case with a very slow time dependence of the bond strength, like that in our experiments.

The fact that the spatial span of the attractive potential is only about 0.25 nm supports a recent conclusion drawn from neutron scattering studies that the stretchable length of a noncovalent bond is rather short, of the order of the diameter of a hydrogen atom (*29*). This short range is also consistent with the 3-D structure of the binding pocket. At a distance of 0.25 nm away from the binding pocket the structural match between the receptor and pocket skeleton no longer exists and thus no more ctB$-G_{M1}$ bond (*9*, *10*). Therefore, the binding between ctB and its receptor, and possibly in general any ligand−receptor bindings of noncovalent nature, is governed by an attractive potential of deep depth and a rather short spatial span. The short-range attraction makes the specificity more prominent in most ligand−receptor bindings in which a structural match between the receptor and its binding pocket plays a more important role than the overall environment such as ionic strength and species.

The meaning of this short spatial span is that on average the bond surely breaks if it is stretched to this length. However, as a force is applied, the conformation of the protein may also be altered because of the stretching, so that the total stretching of the protein can be actually larger than the bond stretching. In our experiments, the spring force of the cantilever determines the magnitude of the binding force. The stretching of the cantilever is much larger than the stretching of the protein and the bond combined, because of the much smaller spring constant of the cantilever (0.06 vs 1.6 N/m), so that the bond stretching is not directly measured. Instead, it is determined through the fitting. It is preferable to directly measure the stretching of the bond, but then the differentiation of the bond stretching from the protein stretching due to conformational changes may still be problematic. Besides, if one uses a much harder cantilever, the instrumental sensitivity must also be significantly improved from the current level for the detection of the same magnitude forces. However, it is possible in the future to achieve the goal of directly measuring the combined stretching of the protein and bond with technology developments and then open avenues for researchers to differentiate protein stretching and bond stretching to directly measure the stretched length of the bond.

The ctB$-G_{M1}$ bond strength does not have any systematic time dependence, as shown in Figure 5. We can examine the situation in a different perspective by a plot of the average bond strength vs frequency with error bars shown (Figure 7). The frequency range of 0.1−10 Hz in our experiments corresponds to a tip−sample contact time of about 10 ms to 1 s. This does not rule out the possible time dependence at time scales outside this window. It may also be that the actual time dependence is a rather slow varying function so that a time window of two decades is still not significant to show any effect beyond the experimental error. This situation is in contrast to that of the biotin−streptavidin bond, where the use of BFP resulted in a systematic time dependence of

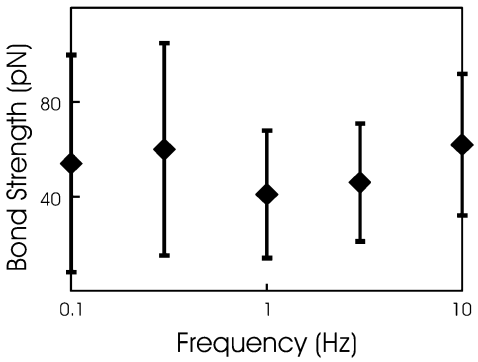

FIGURE 7: Plot of average bond strength with the standard deviation error bar vs vertical raster frequency. The bond strength is in pN.

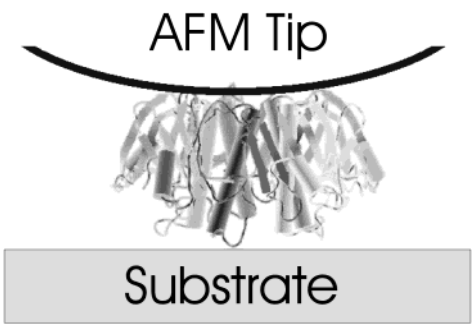

FIGURE 8: Model depicting actual molecular perspectives of the sandwich structure with tip-bound ctB between the tip and the substrate.

the bond strength distribution functions (*18*). In their study, they pointed out the similarity of the average bond strength at loading rates comparable to that of earlier AFM investigations (*13*, *30*). However, the distribution functions of the two cases are markedly different. The experiments with BFP on the measurements of the biotin−streptavidin bond showed a very broad distribution function at loading rates close to that operating of an AFM (*18*). In contrast, the earlier experiments with AFM did show well-defined distribution functions (*13*, *30*). No explanation was given about this difference by Merkel et al. According to the single bond molecular dynamics model, the distribution function at loading rates close to that of AFM is rather broad, with standard deviation intrinsically even much broader than the maximum value, leading to a much less defined meaning of any average value. In view of the model, it is conceivable that the theory may be more appropriate when it predicts a well-defined distribution function. When it reaches the limit resulting in a very broad distribution function, the model may not be suitable to describe the system.

It is also worth examining structural characteristics of the environments around ligand−receptor bonds in different experiments. For the biotin−streptavidin bond measured by BFP, the bond was connected to a rather long soft polymer (PEG) (*18*). For the much earlier measurements, polymeric beads, instead of a single polymer strand, were used (*13*, *30*). For another case showing systematic time dependence with the P-selectin−PSGL-1 bond, rather soft biomolecules, IgG, were used to bridge the connection of the bond to both the substrate and the tip (*31*). In our case, ctB was directly attached to an AFM tip, and the receptor is incorporated into the substrate. Therefore, for the two cases with systematic time dependence of the bond strength, there were soft elastic materials in direct contact with the weakest link, the ligand−receptor bond that was eventually broken under the pulling force. These bridging materials are effectively soft springs. Intuitively, it is hard to picture how these springs would affect the strength of the bond. However, the energy landscape is certainly changed. These soft springs will make the binding potential to have a much larger spatial span. Thus, although the depth of the potential well is still determined by the strength of the of the ligand−receptor bond, the width of the potential well is, possibly greatly, broadened by the soft bridging materials. The broadening of the potential makes the energy landscape much more susceptible to an external force field. It is possible that time dependence of bond breakage is more profound with a broader potential well. A thorough analysis of the situation needs developments in modeling to take into account the effect of the width of the potential well. Most current theories are mainly concerned with the energetics and, hence, the depth of the binding potential (*28*, *32*).

In our force measurements, the cantilever was pressed against the sample for a force up to about 3 nN, allowing to obtain a good slope, crucial for accurate measurement of the bond strength with the automatic program. It has been reported that a covalent bond could only sustain a pulling force as large as about 2−4 nN (*12*). Would the compression be too large to cause any sample damage? Figure 8 shows the scenario in our experiments. Because the average radius of curvature of an AFM tip is much larger than the dimension of a ctB pentamer, effectively the attached ctB is sandwiched between the tip and the substrate after the tip engagement. So the question becomes, will the ctB be distorted too severely? It can be seen that a ctB monomer has six β-strands and one α-helix spanning the region between the two sandwich surfaces, the substrate and the AFM tip. The five α-helices of the pentamer apparently stand out to initiate the contact between the treated tip and the substrate. The mechanical support for an α-helix is mainly due to hydrogen bonds. The spring constant for a hydrogen bond is about 12 N/m (*33*, *34*). For an α-helix of 11 residues, the overall effective spring constant is about 20 N/m, because of the parallel arrangement of a number of individual H-bonds (*35*). The main α-helix in ctB has 20 residues and thus has a spring constant of about 11 N/m. Then, the five α-helices in the ctB pentamer have a combined spring constant of 55 N/m. Under a force of 3 nN, they would be compressed a net 0.05 nm, much smaller than the dimension of the molecule, and we expect the molecule to respond to the compression elastically. Moreover, a β-strand is much stronger than an α-helix. The spring constant for a normal β-strand is mainly determined by the vibration mode of covalent bonds and hence is rather high. Typical vibration modes of covalent bonds range from 1000 to 4000 cm^{-1} (*36*), with an average mass of amino acids of about 0.135 kDa; the lowest spring constant of a covalent bond is about 16 kN/m. Thus, for β-strands of about 8−10 residues, such as those six strands spanning the space between the tip−substrate sandwich, the average spring constant for each strand is about 2 kN/m. Therefore, a force of 3 nN results in a negligible deformation for any of these six β-strands, should it so happen that these β-strands are in direct contact with the substrate surface. Thus, under compression, the force has been shared by a great number of bonds so that a serious damage to the molecule requires a much larger force, in sharp contrast to

the case of stretching where the force is propagated through each bond so that the weakest link would break. Therefore, in our experiments, the sandwiched ctB molecule should remain intact throughout the force measurements as long as it is not dehydrated.

We note that our results show the promise of using a molecular probe to investigate activities of bacterial toxins. Monoclonal antibodies against cholera toxin have shown specific effects on the binding of ctB to G_{M1} (*37*), and a natural extension of the present work is to see how the presence of antibodies affects the ctB−G_{M1} binding strength. It is also possible to combine the molecular force probe with the molecular engineering approach to study the effect of heteropentamers (*37*, *38*). It is certain that the use of the molecular force probe will obtain useful information in complement to biochemical and biological studies.

In summary, we have shown that the advantage of AFM being a sensitive force probe and our development of an automated data analysis program allow us to elucidate the molecular detail of a specific binding between the bacterial toxin, cholera toxin, and its receptor. Our results demonstrate that even at the molecular level the law of statistical physics still governs the binding and provide the key parameters of the binding potential.

ACKNOWLEDGMENT

We thank Daichun Du for technical assistance and K. Chu for introduction of the VMD program. We are especially grateful for helpful discussions with D. Harries, E. Mertz, D. Rau, A. V. Parsegian, and G. Hummer.

REFERENCES

1. Hanggi, P., Talkner, P., and Borkovec, M. (1990) *Rev. Mod. Phys. 62*, 251−341.
2. Holmgren, J. (1981) *Nature 292*, 413−417.
3. Spangler, B. D. (1992) *Microbiol. Rev. 56*, 622−647.
4. Fishman, P. H. J. (1982) *Membrane Biol. 69*, 85−97.
5. King, C. A., and van Heyningen, W. E. (1973) *J. Infect. Dis. 127*, 639−647.
6. Kuziemko, G. M., Stroh, M., and Stevens, R. C. (1996) *Biochemistry 35*, 6375−6384.
7. Holmgren, J., Elwing, H., Fredman, P., Strannegard, O., and Svennerholm, L. (1979) *Adv. Exp. Med. Biol. 125*, 453−470.
8. Fishman, P. H., Moss, J., and Osborne, J. C., Jr. (1978) *Biochemistry 17*, 711−716.
9. Merritt, E. A., Sarfaty, S., ven der Akker, F., L'Hoir, C., Martial, J. A., and Hol, W. G. J. (1994) *Protein Sci. 3*, 166−175.
10. Zhang, R.-G., Westbrook, M. L., Westbrook, E. M., Scott, D. L., Otwinowski, Z., Maulik, P. R., Reed, R. A., and Shipley, G. G. (1995) *J. Mol. Biol. 251*, 550−562.
11. Shao, Z., and Yang, J. (1995) *Q. Rev. Biophys. 28*, 195−251.
12. Grandbois, M., Beyer, M., Rief, M., Clausen-Schaumann, H., and Gaub, H. E. (1999) *Science 283*, 1727−1730.
13. Moy, V. T., Florin, E. L., and Gaub, H. E. (1994) *Science 266*, 257−260.
14. Boland, T., and Ratner, B. D. (1995) *Proc. Natl. Acad. Sci. U.S.A. 92*, 5297−5301.
15. Hoh, J. H., Cleveland, J. P., Prater, C. B., Revel, J. P., and Hansma, P. K. (1992) *J. Am. Chem. Soc. 114*, 4917−4918.
16. Lee, G. U., Chrisey, L. A., and Colton, R. J. (1994) *Science 266*, 771−773.
17. Marszalek, P. E., Oberhauser, A., Pang, Y. P., and Fernandez, J. M. (1998) *Nature 396*, 661−664.
18. Merkel, R., Nassoy, P. A., Leung, A., Ritchie, K., and Evans, E. (1999) *Nature 397*, 50−53.
19. Fang, Y., Cheley, S., Baylay, H., and Yang, J. (1997) *Biochemistry 36*, 9518−9522.
20. Yang, J., and Appleyard, J. (2000) *J. Phys. Chem. 104*, 8097−8100.
21. Baba, Y., Matsuura, T., Wakamoto, K., Morita, Y., Nishitsu, Y., and Tsuhako, M. (1992) *Anal. Chem. 64*, 1221−1226.
22. Gelbart, W. M., Bruinsma, R. F., Pincus, P. A., and Parsegian, V. A. (2000) *Phys. Today 53*(9), 38−44.
23. Brenner, S. L., and Parsegian, V. A. (1974) *Biophys. J. 14*, 327−334.
24. Thompson, T. E., and Tillack, T. W. (1985) *Annu. Rev. Biophys. Biophys. Chem. 14*, 361−386.
25. Ulrich-Bott, B., and Wiegandt, H. (1984) *J. Lipid Res. 25*, 1233−1245.
26. Lis, L. J., McAlister, M., Fuller, N., Rand, R. P., and Parsegian, V. A. (1982) *Biophys. J. 37*, 657−666.
27. Evans, E., and Ritchie, K. (1997) *Biophys. J. 72*, 1541−1555.
28. Evans, E. (2001) *Annu. Rev. Biophys. Biomol. Struct. 30*, 105−128.
29. Zaccai, G. (2001) *Science 288*, 1604−1607.
30. Florin, E. L., Moy, V. T., and Gaub, H. E. (1994) *Science 264*, 415−417.
31. Fritz, J., Katopodis, A. G., Kolbinger, F., and Anselmetti, D. (1998) *Proc. Natl. Acad. Sci. U.S.A. 95*, 12283−12288.
32. Hummer, G., and Szabo, A. (2001) *Proc. Natl. Acad. Sci. U.S.A. 98*, 3658−3661.
33. Chou, K.-C. (1985) *Biophys. J. 48*, 289−297.
34. Itoh, K., and Shimanouchi, T. (1970) *Biopolymers 9*, 383−399.
35. Chou, K.-C. (1984) *Biophys. J. 45*, 881−890.
36. Cantor, C. R., and Schimmel, P. R., Eds. (1980) *Biophysical Chemistry: part II. Techniques for the study of biological structure and function*, W. H. Freeman, New York.
37. Jobling, M. G., and Holmes, R. K. (2002) *Infect. Immun. 70*, 1260−1271.
38. Tamplin, M. L., Ahmed, M. K., Jalali, R., and Colwell, R. R. (1989) *J. Gen. Microbiol. 135*, 1195−1200.

BI027016H